toxics

MDPI

Article

Theoretical Calculation on the Reaction Mechanisms, Kinetics and Toxicity of Acetaminophen Degradation Initiated by Hydroxyl and Sulfate Radicals in the Aqueous Phase

Mengmeng Xu [1], Junfang Yao [1], Simei Sun [2], Suding Yan [3] and Jingyu Sun [1,*]

[1] Hubei Key Laboratory of Pollutant Analysis & Reuse Technology, College of Chemistry and Chemical Engineering, Hubei Normal University, Cihu Road 11, Huangshi 435002, China; xumm@stu.hbnu.edu.cn (M.X.); yaojf@stu.hbnu.edu.cn (J.Y.)
[2] Huangshi Key Laboratory of Photoelectric Technology and Materials, College of Physics and Electronic Science, Hubei Normal University, Huangshi 435002, China; simeisun@hbnu.edu.cn
[3] College of Urban and Environmental Sciences, Hubei Normal University, Huangshi 435002, China; yansd@hbnu.edu.cn
* Correspondence: sunjy@hbnu.edu.cn; Tel./Fax: +86-0714-6515602

Abstract: The •OH and $SO_4^{\bullet-}$ play a vital role on degrading pharmaceutical contaminants in water. In this paper, theoretical calculations have been used to discuss the degradation mechanisms, kinetics and ecotoxicity of acetaminophen (AAP) initiated by •OH and $SO_4^{\bullet-}$. Two significant reaction mechanisms of radical adduct formation (RAF) and formal hydrogen atom transfer (FHAT) were investigated deeply. The results showed that the RAF takes precedence over FHAT in both •OH and $SO_4^{\bullet-}$ with AAP reactions. The whole and branched rate constants were calculated in a suitable temperature range of 198–338 K and 1 atm by using the KiSThelP program. At 298 K and 1 atm, the total rate constants of •OH and $SO_4^{\bullet-}$ with AAP were 3.23×10^9 M^{-1} s^{-1} and 4.60×10^{10} M^{-1} s^{-1}, respectively, considering the diffusion-limited effect. The chronic toxicity showed that the main degradation intermediates were harmless to three aquatic organism, namely, fish, daphnia, and green algae. From point of view of the acute toxicity, some degradation intermediates were still at harmful or toxic level. These results provide theoretical guidance on the practical degradation of AAP in the water.

Keywords: acetaminophen (AAP); density functional theory; degradation mechanisms; rate constants; acute toxicity; chronic toxicity

Citation: Xu, M.; Yao, J.; Sun, S.; Yan, S.; Sun, J. Theoretical Calculation on the Reaction Mechanisms, Kinetics and Toxicity of Acetaminophen Degradation Initiated by Hydroxyl and Sulfate Radicals in the Aqueous Phase. *Toxics* **2021**, *9*, 234. https://doi.org/10.3390/toxics9100234

Academic Editors: Ruijuan Qu and Zunyao Wang

Received: 18 August 2021
Accepted: 21 September 2021
Published: 25 September 2021

1. Introduction

The problem of water pollution caused by the drug residues have been paid much more attention. Even though the content of these drugs in the water environment is very low, they brings potential dangers to human health and ecological environment due to its strong persistence, bioaccumulation and slow biodegradation [1,2]. Acetaminophen (AAP), as one kind of antipyretic analgesics, enters to water environment by the excretion of humans and animals. The concentration of AAP rose to 6 μg/L in European STP effluents [3]. Its concentration up to 10 μg/L was detected in natural waters in the United States [4], and over 65 μg/L concentration was measured in the Tyne river in the United Kingdom [5]. The removal of micropollution is challenging for water treatment technology. Researches on this area were also relatively limited.

Advanced oxidation processes (AOPs) are highly efficient engineering technologies in the elimination of water micropollutants. The active free radicals (i.e., •OH and $SO_4^{\bullet-}$) generating in AOPs can decompose these contaminants. The ultraviolet/hydrogen peroxide (UV/H_2O_2), Fenton (H_2O_2/Fe^{2+}) and Photo-Fenton (UV/H_2O_2/Fe^{2+}) processes can contribute to •OH, which is shown in the following equation:

$$Fe^{2+} + H_2O_2 \rightarrow Fe^{3+} + \bullet OH + HO^-$$

•OH could be generated from hydrogen peroxide activated by electrochemical process with Fe^{2+}/Fe^{3+}, which can degrade pentachlorophenol (PCP) [6]. The removal of carbamazepine (CBZ) was attributed to •OH formed by coupling H_2O_2 with UV and Fe^{2+}/Fe^{3+} [7]. The removal efficiency of three AOP systems has been compared and found the order of $O_3/H_2O_2/Fe^{2+}$ > $UV/H_2O_2/Fe^{2+}$ > H_2O_2/Fe^{2+} [8]. Certainly, other processes such as photocatalysis and photoelectrocatalysis are able to produce •OH [9].

Meanwhile, the ultraviolet/persulfate ($UV/S_2O_8^{2-}$) can generate $SO_4^{\bullet-}$, which is described by the following equation [10]:

$$S_2O_8^{2-} \xrightarrow{h\nu} SO_4^{\bullet-} + SO_4^{\bullet-}$$

Surely, •OH can be produced when $SO_4^{\bullet-}$ reacts with H_2O, which is presented by the following equation [11]:

$$SO_4^{\bullet-} + H_2O \rightarrow SO_4^{2-} + \bullet OH + H^+$$

Thus, •OH-mediated and $SO_4^{\bullet-}$-mediated degradation of contaminants were available. The redox potential and rate constants are summarized in Table 1. It was reported that the •OH-initiated degradation rate constant was about 10^8–10^{10} M^{-1} s^{-1}. The $SO_4^{\bullet-}$-initiated rate constant was about 10^7–10^{10} M^{-1} s^{-1} [12]. The degradation rates of two reactive radicals are nearly equivalent, which is consistent with their high redox potential (2.5–3.1 V for $SO_4^{\bullet-}$ versus 1.8–2.7 V for •OH) [13–15]. The degradation processes of contaminants triggered by •OH and $SO_4^{\bullet-}$ were investigated in recent years. For example, Tong et al. determined the rate constants of syringic acid reactions with •OH and $SO_4^{\bullet-}$ in aqueous phase by laser flash photolysis. They found that •OH and $SO_4^{\bullet-}$ possessed similar reaction rate at the same pH [16]. Gao et al. measured the rate constants of neutral sulfamethoxazole with •OH and $SO_4^{\bullet-}$ were $(7.27 \pm 0.43) \times 10^9$ and $(2.98 \pm 0.32) \times 10^9$ M^{-1} s^{-1} in the systems of UV/H_2O_2 and UV/PS, respectively [17]. Similarly, Wang et al. detected the rate constants for AAP with •OH and $SO_4^{\bullet-}$ reactions were $(3.26 \pm 0.41) \times 10^9$ and $(1.80 \pm 0.17) \times 10^9$ M^{-1} s^{-1} in the Fe^{2+}/persulfate system, respectively [18]. The second-order rate constants of •OH and $SO_4^{\bullet-}$ were conformed as 5.15×10^9 and 7.66×10^9 M^{-1} s^{-1}, respectively, using the ultraviolet light emitting diode (UV-LED)-based method by Li et al. [19]. However, the study of degradation mechanisms of •OH and $SO_4^{\bullet-}$ with the target contaminants still faced with great challenge. At atom level, quantum chemistry calculation was a powerful tool to gain a in-depth understanding for mechanisms and kinetics of •OH and $SO_4^{\bullet-}$ reacting with some pollutants [20–23].

Table 1. Redox potential and kinetic data for the reactions of •OH and $SO_4^{\bullet-}$.

Radicals	Redox Potential [a] (V)	The Range of Rate Constants [b] (M^{-1} s^{-1})	The Second-Order Rate Constants of Neutral Sulfamethoxazole [c] (M^{-1} s^{-1})	The Second-Order Rate Constants of Acetaminophen (M^{-1} s^{-1})	
				Fe^{2+}/PS [d]	UV-LED/H_2O_2 [e]
•OH	1.8–2.7	10^8–10^{10}	$(7.27 \pm 0.43) \times 10^9$	$(3.26 \pm 0.41) \times 10^9$	5.15×10^9
$SO_4^{\bullet-}$	2.5–3.1	10^7–10^{10}	$(2.98 \pm 0.32) \times 10^9$	$(1.80 \pm 0.17) \times 10^9$	7.66×10^9

[a] (Xiao, et al., 2020; Devi, et al., 2016; Ghanbari, et al., 2017); [b] (Li, et al. 2020, [12]); [c] (Gao, et al., 2020); [d] (Wang, et al., 2019); [e] (Li, et al., 2020, [19]).

Theoretical studies are essential for discussing the degradation processes of AAP with •OH and $SO_4^{\bullet-}$. Therefore, the reaction mechanisms and kinetics of the AAP with •OH and $SO_4^{\bullet-}$ have been studied by using quantum chemistry calculations. Rate constants of every possible pathways for AAP with •OH and $SO_4^{\bullet-}$ reactions were calculated. Even more importantly, the ecotoxicity of AAP and its degradation products has been evaluated in order to know their risk.

2. Computational Methods

2.1. Mechanism Calculation

Usually, reaction mechanisms are investigated by Density functional theory (DFT). M06-2X functional can solve noncovalent interactions for some complexes better than other density functional such as B3LYP [24]. The functional ratio of exchange correction of M06-2X is 54% which will obtain more accurate energies [25]. Furthermore, M06-2X method [26] of DFT was selected in the reactions of AAP with •OH and $SO_4^{\bullet-}$ without hesitation, because satisfactory results were acquired on the degradation of some micropollutants [27–30]. For example, the thermodynamic and kinetic data for ibuprofen reactions with hydroxyl and sulfate radicals reported by Yang et al. were calculated with M06-2X method [27]. All electronic structures and energy calculations were performed using Gaussian 09 software [31]. The reactants (R), transition states (TS) and intermediates (IM) were optimized at the M06-2X/6-31+G(d,p) level. IM (all positive frequencies) and TS (only one imaginary frequency) are primarily identified by harmonic vibration frequency analysis. Moreover, the method of intrinsic reaction coordinates (IRC) was applied to determine every right transition state [32]. The water solvent effect was taken into account by a universal solvation model (SMD) [33] when these structures were optimized in the aqueous phase. Based on right structures, the single point energies were calculated accurately at high level of M06-2X/6-311++G(3df, 2p).The Gibbs free energy barrier of activation ($\Delta G^{\neq}$) and free energy of reaction (ΔG) are calculated as follows:

$$\Delta G^{\neq} = G_{TS} - G_R$$

$$\Delta G = G_{IM} - G_R$$

2.2. Kinetic Calculation

The conventional Transition State Theory (TST) was used to calculate the rate constants implemented by KiSThelP program [34] that has obtained accurate results for contaminants with free radicals reactions [35–39]. The calculation formula is employed in KiSThelP:

$$k = \kappa\sigma\frac{k_b T}{h}\left(\frac{RT}{P^0}\right)^{\Delta n} e^{-\frac{\Delta G^{0,\neq}}{k_b T}}$$

Some parameters need to be explained. κ is tunneling correction factor of Wigner approach [34]. σ, k_b and h are the reaction path degeneracy, Boltzmann's constant and Planck's constant, respectively. $\Delta G^{0,\neq}$ is the standard Gibbs free energy of activation. RT/P^0 has the unit of the inverse of a concentration. For bimolecular reactions, Δn is equal to 1.

The diffusion-limited effect was considered to obtain the apparent rate constants (k_{app}) of aqueous phase based on Collins-Kimball theory [40].

$$k_{app} = \frac{k_{aq}k_D}{k_{aq} + k_D}$$

where, k_{aq} is calculated by TST as aqueous rate constant. k_D is calculated by the Smoluchowski equation as the diffusion-limited rate constants:

$$k_D = 4\pi R_{AB} D_{AB} N_A$$

R_{AB} means the reaction distance, and N_A is Avogadro's number, D_{AB} represents the sum of diffusion coefficient of the reactants A (AAP) and B (•OH or $SO_4^{\bullet-}$). The calculations of D_A and D_B are realized by using the Stokes–Einstein approach [41]:

$$D = \frac{k_b T}{6\pi\alpha\eta}$$

where k_b, T, η, and α are the Boltzmann constant, temperature, viscosity of the solvent, and radius of the solute, respectively. For water, $\eta = 8.9 \times 10^{-4}$ Pa s.

2.3. Ecotoxicity Calculation

The aquatic toxicity of AAP and its degradation products was evaluated by using the Structure Activity Relationship (SAR) method with the ECOSAR program [42], which has

been successfully used to evaluate the acute and chronic toxicity [43–46]. Three aquatic organisms of green algae, daphnia and fish were considered to assess the acute and chronic toxicities. Acute toxicity of the target compounds was estimated by median lethal concentration (LC50) and median effect concentration (EC50). LC50 is defined 50% lethal concentration for fish and daphnia in 96 and 48 h, respectively. EC50 is 50% effective concentration for green algae in 96 h. The chronic toxicity was described by the chronic toxicity value (ChV) for green algae, daphnia and fish.

3. Results and Discussion

3.1. Degradation Mechanisms

The degradation mechanisms of AAP initiated by •OH and $SO_4^{\bullet-}$ mainly include radical adduct formation (RAF) and formal hydrogen atom transfer (FHAT). Similarities and differences of mechanisms about two reactions were adequately investigated. The Gibbs free energy of reaction (ΔG) and Gibbs free energy barrier of activation ($\Delta G^{\neq}$) of the initial reaction of AAP with •OH and $SO_4^{\bullet-}$ were calculated and discussed. The binding distances and angles of AAP, •OH and $SO_4^{\bullet-}$ are shown in Figure 1. All structures of transition states are plotted in Figure S1 (Supplementary Materials).

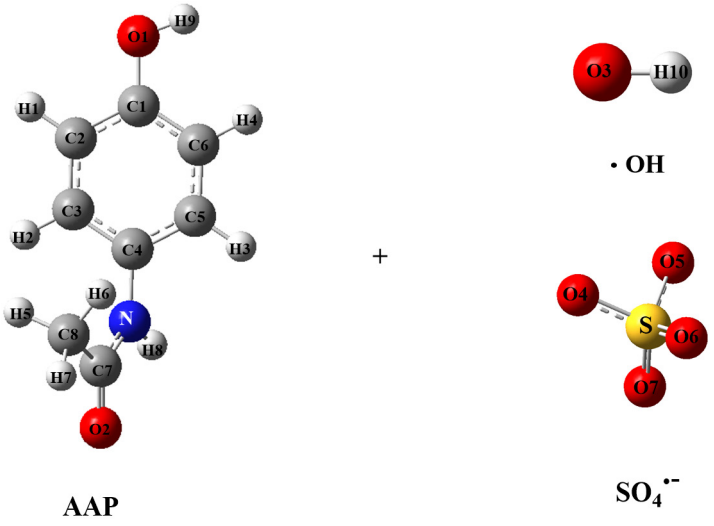

	distance(Å)		distance(Å)		Angle(°)
O1-H9	0.968	N-H8	1.016	∠H9-O1-C1	110.22°
C1-O1	1.372	N-C7	1.353	∠O1-C1-C2	117.38°
C1-C2	1.395	C7-O2	1.242	∠C1-C2-H1	119.48°
C2-C3	1.391	C7-C8	1.504	∠C4-N-H8	117.29°
C3-C4	1.397	C8-H5	1.094	∠H8-N-C7	114.98°
C4-C5	1.395	C8-H6	1.091	∠C8-C7-O2	121.06°
C5-C6	1.392	C8-H7	1.090	∠H6-C8-H7	110.19°
C6-C1	1.395	O3-H10	0.978	∠O5-S-O6	112.18°
C2-H1	1.085	S-O4	1.528	∠O4-S-O5	92.18°
C3-H2	1.085	S-O5	1.528	∠O6-S-O7	113.99°
C5-H3	1.086	S-O6	1.466		
C6-H4	1.086	S-O7	1.466		
C4-N	1.424				

Figure 1. The structures of AAP, •OH and $SO_4^{\bullet-}$ calculated at the M06-2X/6-31 + G(d,p) level. The bond distance (Å) and angles (°) are listed. Here, =H =C =O =S =N.

3.1.1. Radical Adduct Formation

RAF pathways of AAP with •OH and $SO_4^{\bullet-}$ reactions are displayed in Figure 2. •OH-initiated and $SO_4^{\bullet-}$-initiated RAF channels consist of addition on the benzene ring and the acetamide group. It is uniform for the RAF mechanisms of AAP with •OH and $SO_4^{\bullet-}$ reactions. The acetamide group addition has no advantage over that of the benzene ring because the free energy barriers are 15.23 and 30.86 kcal/mol for acetamide group addition of •OH and $SO_4^{\bullet-}$, respectively. However, the free energy barriers were 5.95–9.26 kcal/mol and 2.66–8.74 kcal/mol for •OH and $SO_4^{\bullet-}$ addition to six carbon atoms of benzene ring, respectively. Generally, •OH-triggered reactions are higher exothermic than that of $SO_4^{\bullet-}$. Based on the values of $\Delta G^{\neq}$ and ΔG, C_6 atom addition (path 6 for •OH-triggered reactions versus path 13 for $SO_4^{\bullet-}$-triggered reactions) is the most favorable channels because their barriers are only 5.95 and 2.66 kcal/mol, respectively. Recently, the similar addition results were proved by Li et al. [47]. Figure 3 shows the comparison of potential energies for RAF mechanisms of two radicals reactions. $SO_4^{\bullet-}$-initiated reactions have the lower free energy barriers than that of •OH. In $SO_4^{\bullet-}$-initiated reactions, TS13, C_6 addition transition state, has stronger hydrogen bond intermolecular interaction, namely, hydrogen atom of phenolic hydroxyl group of AAP with oxygen atom of $SO_4^{\bullet-}$. IRC intuitively shows hydrogen atom of phenolic hydroxyl group of AAP tends to be close to oxygen atom of $SO_4^{\bullet-}$. The interaction will greatly decrease reaction barrier. However, $SO_4^{\bullet-}$-initiated reactions have less reaction heats compared with •OH-initiated reactions. For example, the energy barrier of path 6 is higher 3.29 kcal/mol than path 13, but path 6 is more exothermic than 6.95 kcal/mol.

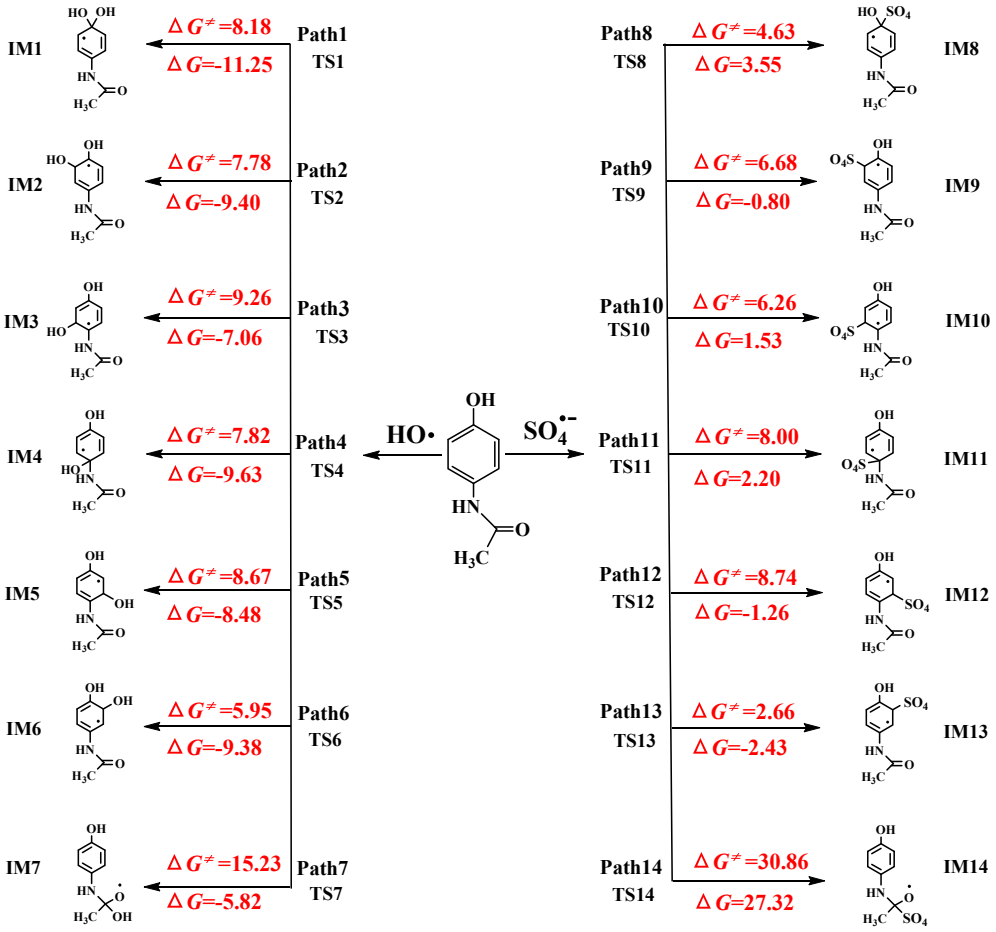

Figure 2. The radical adduct formation channels of AAP with •OH and $SO_4^{\bullet-}$ reactions with the Gibbs free energy of reaction (ΔG) and Gibbs free energy barrier of activation ($\Delta G^{\neq}$) (unit: kcal/mol).

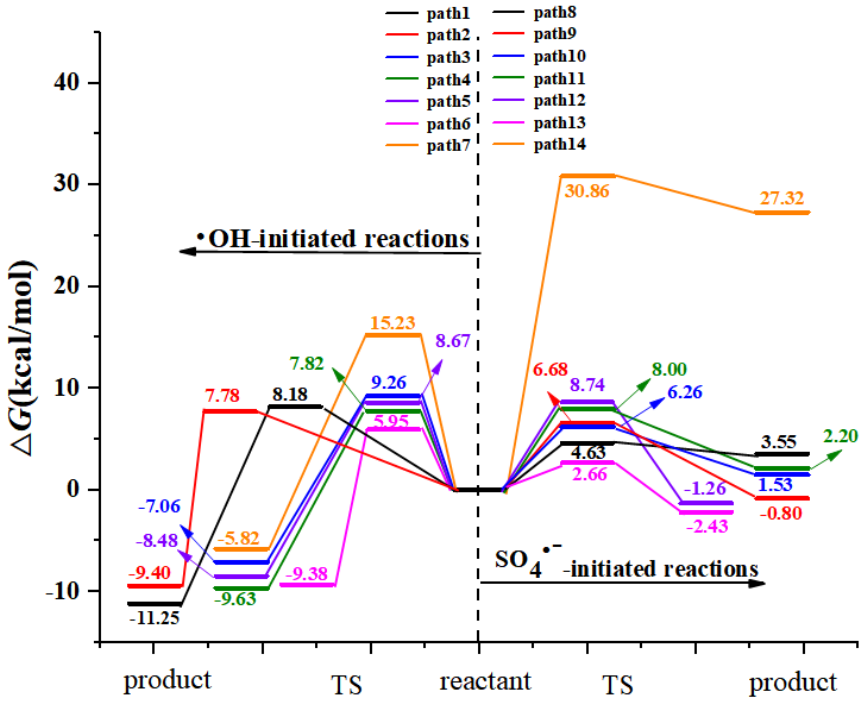

Figure 3. The free energy diagram of RAF pathways initiated by two radicals.

3.1.2. Formal Hydrogen Atom Transfer

Ten hydrogen abstraction pathways from benzene ring and methyl group are found and shown in Figure 4. Hydrogen abstractions from C2, C3, and C5 of benzene ring experience TS15, TS16, TS17 with free energy barriers of 19.13, 18.75 and 19.75 kcal/mol for AAP with •OH reactions, respectively. For $SO_4^{\bullet-}$-initiated reactions, the free energy barriers of hydrogen abstractions from C2, C3, C5, and C6 of benzene ring are 30.58, 19.60, 19.30 and 30.43 kcal/mol, respectively. The hydrogen atom can be abstracted from C_6 of benzene ring and the methyl group via 14.27 and 14.41 kcal/mol barriers for •OH-initiated path 18 and path 19. Moreover, the corresponding products are exothermic 7.02 and 11.37 kcal/mol, respectively. The results indicate that hydrogen abstractions from C_6 of benzene ring and methyl group are two important channels for •OH with AAP reaction. However, methyl group hydrogen abstraction is the most important channel for $SO_4^{\bullet-}$ with AAP reaction due to the lowest energy barrier of 10.91 kcal/mol. Figure 5 describes the comparison of free energies for FHAT mechanisms. As shown in the Figure 5, the free energy barriers for $SO_4^{\bullet-}$ abstracting hydrogen atom from benzene ring are higher than that of •OH, and the corresponding paths (path 20–path 23) initiated by $SO_4^{\bullet-}$ are less exothermic than path 15–path 18 initiated by •OH. However, the free energy barrier of $SO_4^{\bullet-}$-initiated path 24 is lower 3.5 kcal/mol than •OH-initiated path 19, and path 24 is more exothermic 1.76 kcal/mol than path 19.

The comparison of FHAT and RAF mechanisms is shown in Figure 6. It is implied that RAF has an advantage over FHAT for both reactions. The free energy barrier for the most important RAF channel is lower 8.32 and 8.25 kcal/mol than the most favorable FHAT channel for •OH-initiated and $SO_4^{\bullet-}$-initiated reactions, respectively.

3.2. Kinetics

The rate constants involved free radicals reactions are of great value for predicting the degradation rate. However, the measurement of such data is difficult due to these rapid reactions. The theoretical calculations play an important role in attaining rate constants for these radical-participating reactions.

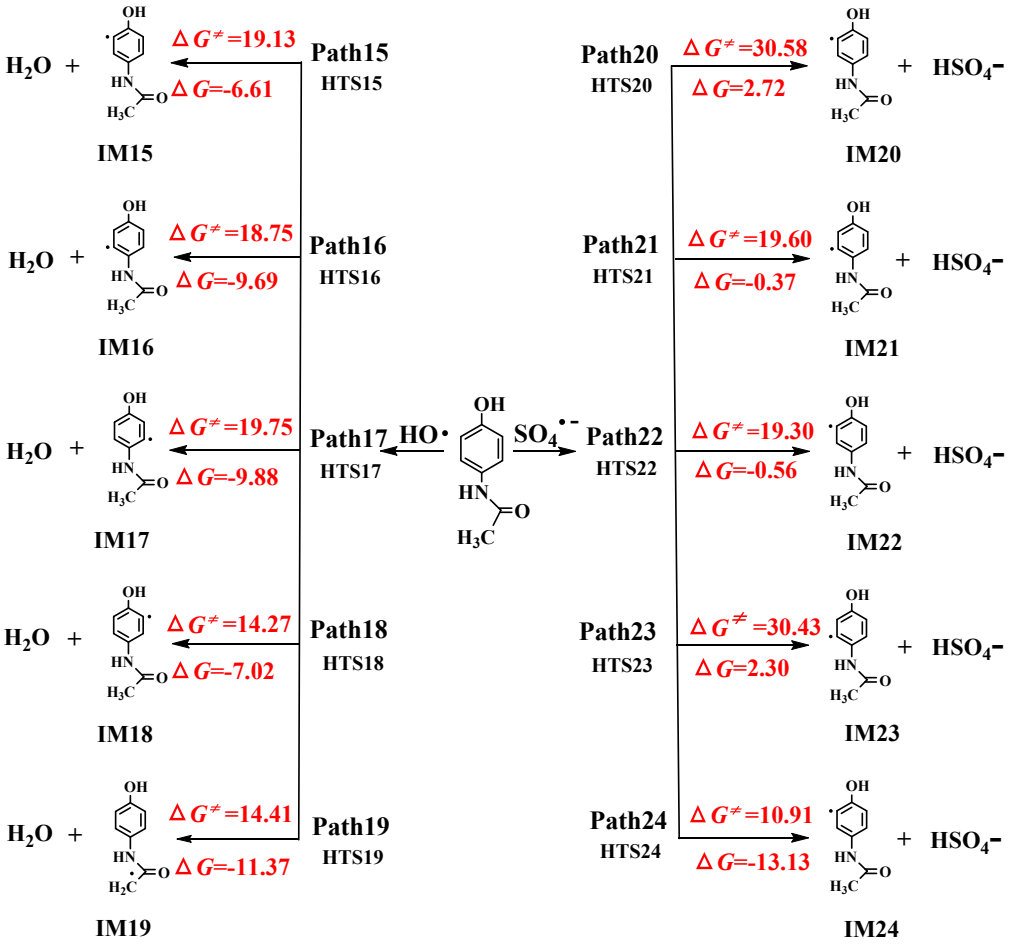

Figure 4. The formal hydrogen atom transfer channels of AAP with •OH and $SO_4^{\bullet-}$ reactions with the Gibbs free energy of reaction (Δ*G*) and Gibbs free energy barrier of activation ($\Delta G^{\neq}$) (unit: kcal/mol).

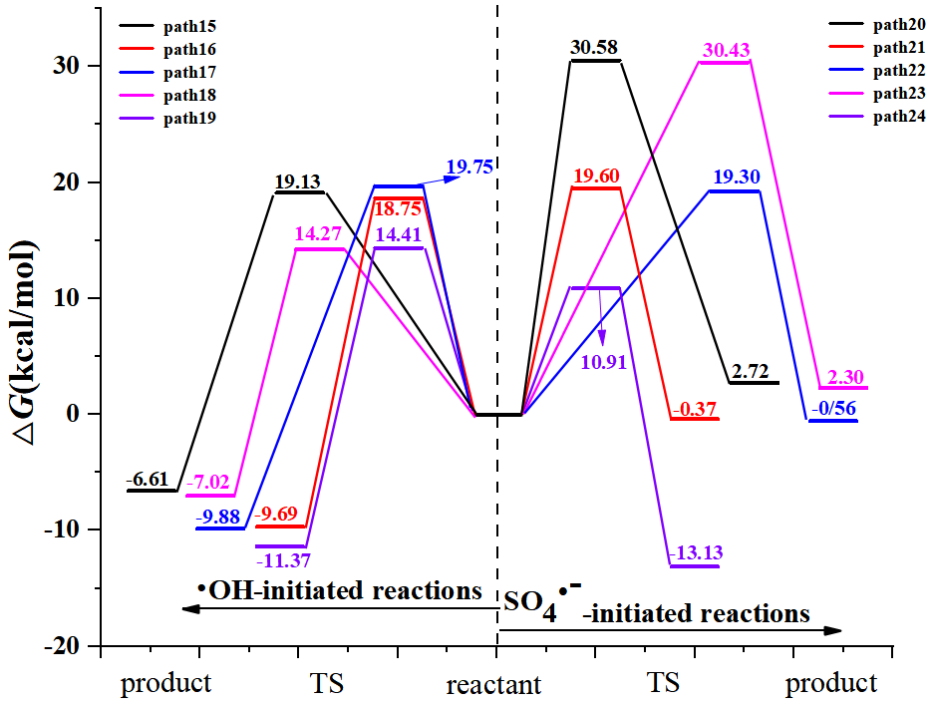

Figure 5. The free energy diagram of FHAT pathways initiated by two radicals in the aqueous phase.

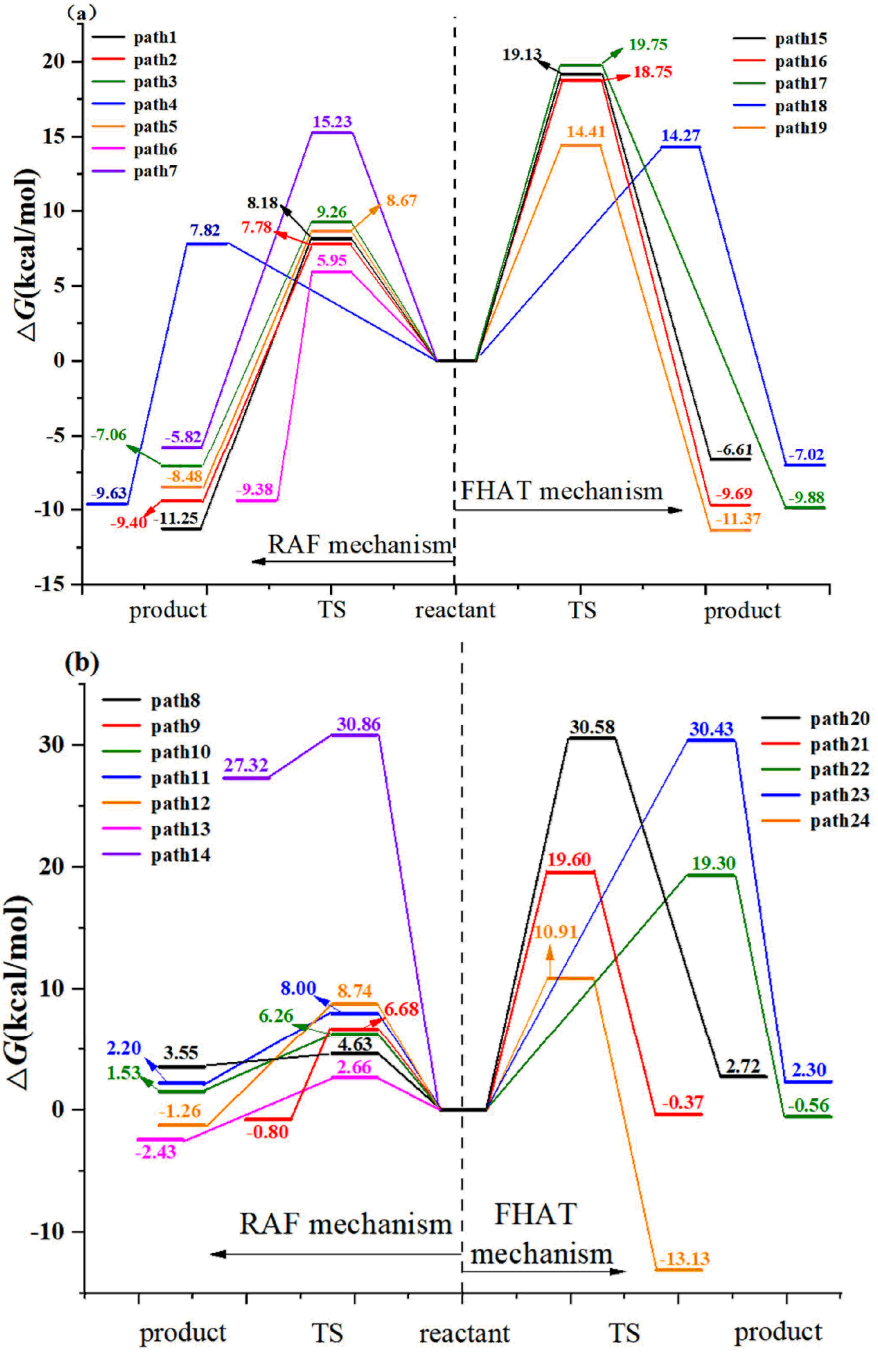

Figure 6. Free energy profiles for FHAT and RAF mechanisms in aqueous phase. (**a**) APP with •OH reactions; (**b**) APP with $SO_4^{\bullet-}$ reactions.

The rate constants for AAP with •OH reactions are given in Table 2. The apparent rate constant of •OH reaction with AAP (k_{app}) is 3.23 × 10^9 M^{-1} s^{-1} at 298 K. The calculated rate constant is consistent with experimental results of (3.26 ± 0.41) × 10^9 and 5.15 × 10^9 M^{-1} s^{-1} [18,19]. The C_6 site addition (path 6) has the largest rate constant of 3.56 × 10^9 M^{-1} s^{-1} with the 84.8% branching ratio. The other RAF and FHAT pathways contribute the total reactions weakly. The rate constants for AAP with $SO_4^{\bullet-}$ reactions are depicted in Table 3. The apparent rate constant of $SO_4^{\bullet-}$ reaction with AAP (k'_{app}) is 4.60 × 10^{10} M^{-1} s^{-1} at 298 K, which is higher six times than experimental value of 7.66 × 10^9 M^{-1} s^{-1} [19]. The possible reason is that the lower barrier leads to higher reaction rate, which agrees with discussion of mechanisms. Theoretical model and method will lead to some deviations, but the accuracy of experiment is affected by some factors such

as equipment, reagent, and operation. Theoretical calculations can predict and explain some results. Consequently, the benefits of theoretical calculations cannot be underestimated. The C_6 site addition (path 13) is dominant channel with the largest rate constant of 8.65×10^{13} M^{-1} s^{-1} that possesses the 92.8% branching ratio. The other RAF and FHAT pathways have a little contribution for AAP with $SO_4^{\bullet-}$ reaction. As shown in Table 4, C_6 of benzene ring and methyl group hydrogen abstractions are dominant channels for •OH with AAP reaction with the branching ratio of 50.42% and 49.58%, respectively. For AAP with $SO_4^{\bullet-}$ reaction, methyl group hydrogen abstraction contributes 100% to FHAT channels.

Table 2. The calculated rate constants(k_{aq}), steady-state rate constant (k_D), apparent rate constant (k_{app}) and branching ratio (R_{aq}) for the AAP with •OH reaction in the aqueous phase at 298 K.

Paths	k_{aq} (M^{-1} s^{-1})	R_{aq} (%)	k_D (M^{-1} s^{-1})	k_{app} (M^{-1} s^{-1})
APP + •OH → IM1 (k_1)	8.04×10^7	1.9	9.80×10^9	7.97×10^7
APP + •OH → IM2 (k_2)	1.87×10^8	4.5	9.80×10^9	1.83×10^8
APP + •OH → IM3 (k_3)	1.51×10^7	0.4	9.80×10^9	1.51×10^7
APP + •OH → IM4 (k_4)	3.22×10^8	7.6	9.80×10^9	3.12×10^8
APP + •OH → IM5 (k_5)	3.33×10^7	0.8	9.80×10^9	3.32×10^7
APP + •OH → IM6 (k_6)	3.56×10^9	84.8	9.80×10^9	2.61×10^9
APP + •OH → IM7 (k_7)	6.75×10^2	0	9.80×10^9	6.75×10^2
APP + •OH → IM15 (k_{15})	4.75	0	9.80×10^9	4.75
APP + •OH → IM16 (k_{16})	9.75	0	9.80×10^9	9.75
APP + •OH → IM17 (k_{17})	1.91	0	9.80×10^9	1.91
APP + •OH → IM18 (k_{18})	1.15×10^4	0	9.80×10^9	1.15×10^4
APP + •OH → IM19 (k_{19})	1.13×10^4	0	9.80×10^9	1.13×10^4
APP + •OH → Product (k_{total})	4.20×10^9	100		3.23×10^9

Table 3. The calculated rate constants(k'_{aq}), steady-state rate constant (k'_D), apparent rate constant (k'_{app}) and branching ratio (R'_{aq}) for the AAP with $SO_4^{\bullet-}$ reaction in the aqueous phase at 298 K.

Paths	k'_{aq} (M^{-1} s^{-1})	R'_{aq} (%)	k'_D (M^{-1} s^{-1})	k'_{app} (M^{-1} s^{-1})
APP + $SO_4^{\bullet-}$ →IM8 (k'_8)	6.00×10^{12}	6.4	8.05×10^9	8.04×10^9
APP + $SO_4^{\bullet-}$ → IM9 (k'_9)	1.61×10^{11}	0.2	8.05×10^9	7.67×10^9
APP + $SO_4^{\bullet-}$ → IM10 (k'_{10})	2.60×10^{11}	0.3	8.05×10^9	7.81×10^9
APP + $SO_4^{\bullet-}$ → IM11 (k'_{11})	3.28×10^{10}	0.01	8.05×10^9	6.46×10^9
APP + $SO_4^{\bullet-}$ → IM12 (k'_{12})	2.52×10^{11}	0.3	8.05×10^9	7.80×10^9
APP + $SO_4^{\bullet-}$ → IM13 (k'_{13})	8.65×10^{13}	92.8	8.05×10^9	8.05×10^9
APP + $SO_4^{\bullet-}$ → IM14 (k'_{14})	1.77×10^{-6}	0	8.05×10^9	1.77×10^{-6}
APP + $SO_4^{\bullet-}$ → IM20 (k'_{20})	14.3	0	8.05×10^9	14.3
APP + $SO_4^{\bullet-}$ → IM21 (k'_{21})	1.11×10^2	0	8.05×10^9	1.11×10^2
APP + $SO_4^{\bullet-}$ → IM22 (k'_{22})	1.88×10^2	0	8.05×10^9	1.88×10^2
APP + $SO_4^{\bullet-}$ → IM23 (k'_{23})	5.55	0	8.05×10^9	5.55
APP + $SO_4^{\bullet-}$ → IM24 (k'_{24})	1.33×10^8	0	8.05×10^9	1.33×10^8
APP + $SO_4^{\bullet-}$ → Product (k'_{total})	9.32×10^{13}	100		4.60×10^{10}

Table 4. The calculated rate constants (k_{aq}, k'_{aq}) and branching ratio (R_{aq}, R'_{aq}) for the formal hydrogen atom transfer channels in the aqueous phase at 298 K.

Paths	k_{aq} (M^{-1} s^{-1})	R_{aq} (%)	Paths	k'_{aq} (M^{-1} s^{-1})	R'_{aq} (%)
APP + •OH (FHAT)	2.28×10^4	100	APP + $SO_4^{\bullet-}$ (FHAT)	1.33×10^8	100
APP + •OH → IM15 (k_{15})	4.75	0	APP + $SO_4^{\bullet-}$ → IM20 (k'_{20})	14.3	0
APP + •OH → IM16 (k_{16})	9.75	0	APP + $SO_4^{\bullet-}$ → IM21 (k'_{21})	1.11×10^2	0
APP + •OH → IM17 (k_{17})	1.91	0	APP + $SO_4^{\bullet-}$ → IM22 (k'_{22})	1.88×10^2	0
APP + •OH → IM18 (k_{18})	1.15×10^4	50.42	APP + $SO_4^{\bullet-}$ → IM23 (k'_{23})	5.55	0
APP + •OH → IM19 (k_{19})	1.13×10^4	49.58	APP + $SO_4^{\bullet-}$ → IM24 (k'_{24})	1.33×10^8	100

The temperature dependence of rate constants is shown in Figure 7 at the temperatures from 198 to 338 K and 1 atm, and the corresponding data are listed in Tables S1 and S2 (Supplementary Materials). The total rate constants have weakly negative temperature dependence for •OH-initiated reaction. However, $SO_4^{\bullet-}$-initiated reactions have distinctly negative temperature dependence.

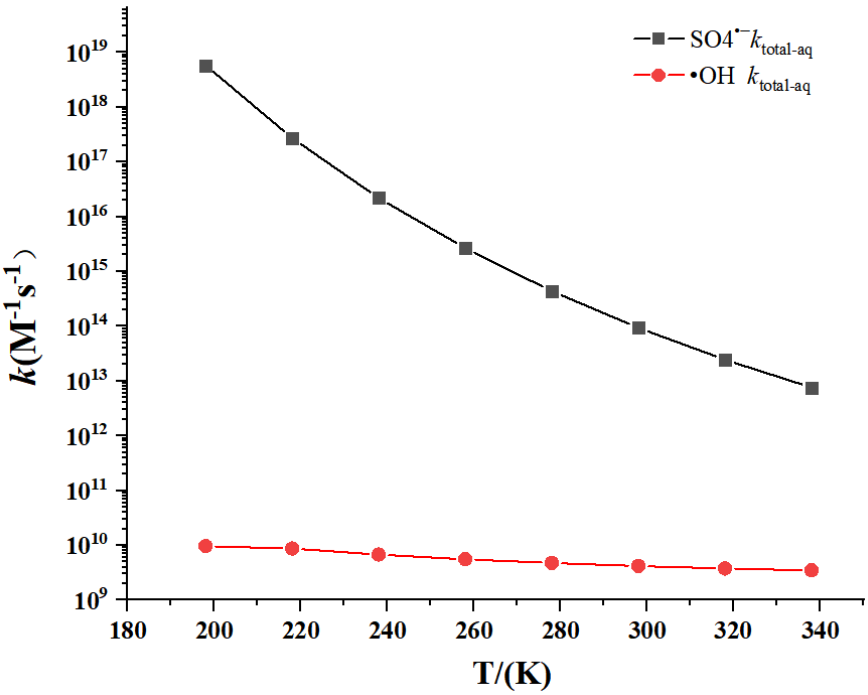

Figure 7. Temperature dependence of the calculated rate constants.

3.3. The Aquatic Toxicities of AAP and Its Degradation Intermediates

The acute and chronic toxicities of AAP and the important degradation intermediates are assessed in three different aquatic organisms, which is drawn in Figure 8. Four types are classified and listed in Table S3 (Supplementary Materials). The toxic values of AAP and the important degradation intermediates are shown in Table S4 (Supplementary Materials).

3.3.1. Toxicity of AAP

The acute toxicity value of AAP is calculated as 323 mg/L of LC50 for fish, 63.1 mg/L of LC50 for daphnia and 26.3 mg/L of EC50 for green algae, respectively. These results indicate that AAP is harmful to daphnia and green algae, but not harmful to fish. The calculated ChV of AAP is 26.3 mg/L for fish, 5.13 mg/L for daphnia, and 37.2 mg/L for green algae. AAP is not harmful to fish and green algae at chronic level. However, it is harmful to daphnia chronically.

3.3.2. Toxicities of the Degradation Products

The most important intermediate (IM6) is harmful to three aquatic organisms in acute toxicity, but is harmless to three aquatic organisms in chronic toxicity. For other degradation intermediates, IM1 is acutely toxic for fish and green algae, and harmful to daphnia. The chronic toxicity of IM1 is harmful for three aquatic organisms. IM13 and IM8 are not harmful for three aquatic organisms chronically. Moreover, IM13 and IM8 are not acutely harmful for fish and daphnia, but pose a severe threat for green algae. In brief, the most important degradation intermediate (IM6) from •OH-initiated reaction is still harmful to aquatic organisms. IM13 from $SO_4^{\bullet-}$-initiated reaction is harmless to fish and daphnia, but is very toxic to green algae. Thus, the toxicity of these compounds should be concerned.

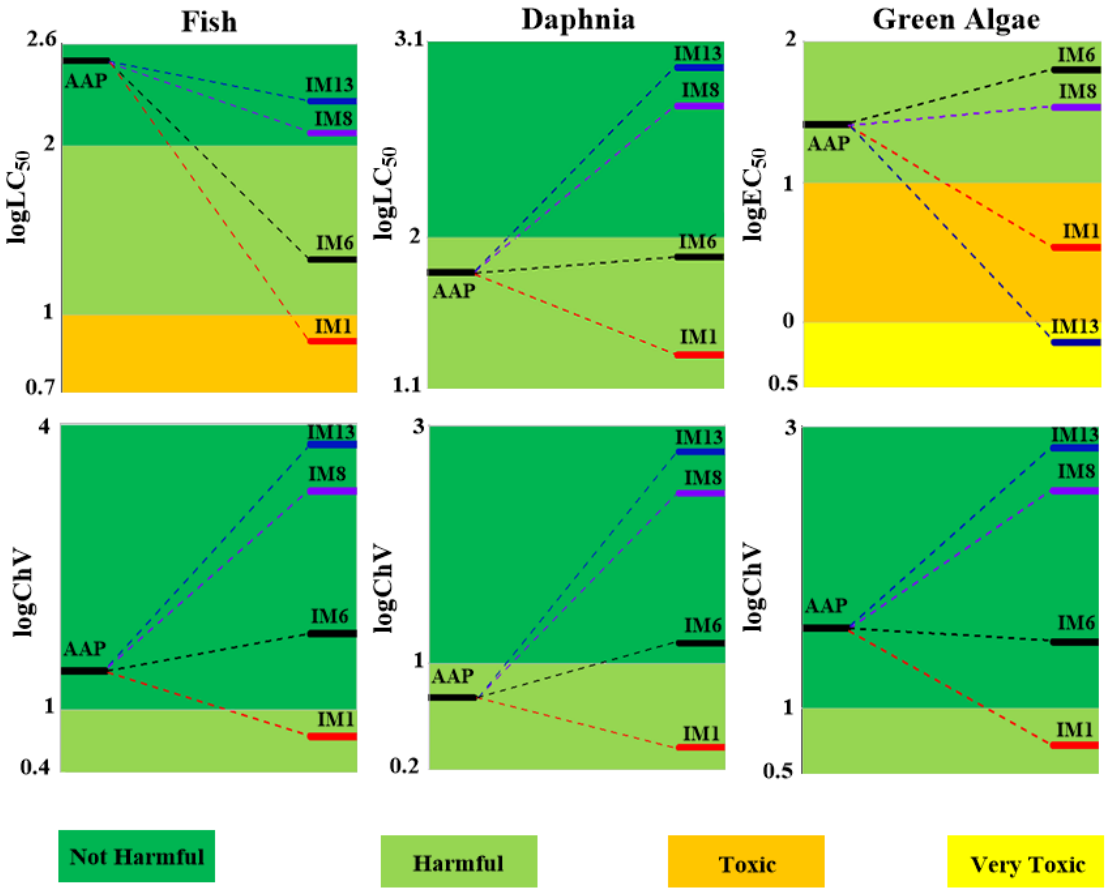

Figure 8. Acute and chronic toxicity (mg/L) of AAP and its transformation intermediates to aquatic organisms (fish, daphnia, and green algae).

4. Conclusions

In this work, the reaction mechanisms and rate of AAP with •OH and $SO_4^{\bullet-}$ have been explored theoretically in aqueous phase. The toxicity of AAP and its transformation intermediates to three aquatic organisms have been assessed. The novelty are summarized as below:

(1) M06-2X/6-311+G (3df, 2p)//M06-2X/6-31+G (d, p) has been used to study the •OH-initiated and $SO_4^{\bullet-}$-initiated transformation mechanism of AAP. •OH and $SO_4^{\bullet-}$ with AAP reactions have the same reaction sites, even reaction mechanisms. The results implied that the C_6 addition is prominent pathway in RAF mechanisms and hydrogen abstraction of methyl group is dominant pathway for both reactions in FHAT mechanism. RAF takes precedence over FHAT.

(2) At 298 K, the total apparent rate constant of AAP with $SO_4^{\bullet-}$ is larger than that of •OH. The calculated rate constants basically matched with experimental values. Theoretical calculations predicted the kinetic data at 198 K–338 K.

(3) Toxic assessment shows that some representative degradation intermediates present an acute threat to the target organisms. Thus, subsequent degradation should be implemented until they are degraded into non-toxic substances.

In brief, this work explains the degradation processes of AAP initiated by •OH and $SO_4^{\bullet-}$ from microscopic points, and solves the problem of structures of intermediates and products which are associated with reactivity. The calculation of eco-toxicity plays an important role on assessing toxicity of degradation process. Finally, these results can apply to the practical degradation of AAP in AOPs.

Supplementary Materials: The following are available online at https://www.mdpi.com/article/10.3390/toxics9100234/s1, Figure S1: Optimized geometries involving the transition states of AAP with •OH and $SO4^{\bullet-}$ at the M06-2X/6-31+G(d,p) level, Table S1: Calculated rate constants of AAP with •OH from 198 to 338 K and 1 atm, Table S2: Calculated rate constants of AAP with $SO4^{\bullet-}$ from 198 to 338 K and 1 atm, Table S3: The acute and chronic toxicity class (mg L^{-1}), Table S4: Eco-toxicity values of AAP and its transformation intermediates to aquatic organisms (mg L^{-1})

Author Contributions: Conceptualization, M.X. and J.Y.; methodology, J.Y.; software, J.S.; validation, S.S., S.Y. and J.S.; formal analysis, M.X.; investigation, M.X.; resources, J.S.; data curation, S.Y.; writing—original draft preparation, M.X.; writing—review and editing, J.Y. and S.S.; visualization, J.Y.; supervision, J.S; project administration, J.S; funding acquisition, J.S. All authors have read and agreed to the published version of the manuscript.

Funding: This research was funded by the National Natural Science Foundation of China, grant number 21507027, and the Natural Science Foundation of Hubei Province, grant number 2020CFB468.

Institutional Review Board Statement: Not applicable.

Informed Consent Statement: Not applicable.

Conflicts of Interest: The authors declare no conflict of interest.

References

1. Akhtar, J.; Amin, N.A.S.; Shahzad, K. A review on removal of pharmaceuticals from water by adsorption. *Desalin. Water Treat.* **2015**, *57*, 12842–12860. [CrossRef]
2. Papageorgiou, M.; Kosma, C.; Lambropoulou, D. Seasonal occurrence, removal, mass loading and environmental risk assessment of 55 pharmaceuticals and personal care products in a municipal wastewater treatment plant in Central Greece. *Sci. Total Environ.* **2016**, *543*, 547–569. [CrossRef]
3. Ternes, T.A. Occurrence of drugs in German sewage treatment plants and rivers. *Water Res.* **1998**, *32*, 3245–3260. [CrossRef]
4. Kolpin, D.W.; Furlong, E.T.; Meyer, M.T.; Thurman, E.M.; Zaugg, S.D.; Barber, L.B.; Buxton, H.T. Pharmaceuticals, hormones, and other organic wastewater contaminants in U.S. streams, 1999–2000: A national reconnaissance. *Environ. Sci. Technol.* **2002**, *36*, 1202–1211. [CrossRef]
5. Roberts, P.H.; Thomas, K.V. The occurrence of selected pharmaceuticals in wastewater effluent and surface waters of the lower Tyne catchment. *Sci. Total Environ.* **2006**, *356*, 143–153. [CrossRef] [PubMed]
6. Govindan, K.; Raja, M.; Noel, M.; James, E.J. Degradation of pentachlorophenol by hydroxyl radicals and sulfate radicals using electrochemical activation of peroxomonosulfate, peroxodisulfate and hydrogen peroxide. *J. Hazard. Mater.* **2014**, *272*, 42–51. [CrossRef] [PubMed]
7. Ali, F.; Khan, J.A.; Shah, N.S.; Sayed, M.; Khan, H.M. Carbamazepine degradation by UV and UV-assisted AOPs: Kinetics, mechanism and toxicity investigations. *Process. Saf. Environ.* **2018**, *117*, 307–314. [CrossRef]
8. Khodadadi, T.; Solgi, E.; Mortazavi, S.; Nourmoradi, H. Comparison of advanced oxidation methods of Fenton, UV/Fenton, and O_3/Fenton in treatment of municipal wastewater. *Desalin. Water Treat.* **2020**, *206*, 108–115. [CrossRef]
9. Collivignarelli, M.C.; Miino, M.C.; Arab, H.; Bestetti, M.; Franz, S. Efficiency and energy demand in polishing treatment of wastewater treatment plants effluents: Photoelectrocatalysis vs. Photocatalysis and photolysis. *Water* **2021**, *13*, 821. [CrossRef]
10. Moussavi, G.; Pourakbar, M.; Aghayani, E.; Mahdavianpour, M. Investigating the aerated VUV/PS process simultaneously generating hydroxyl and sulfate radicals for the oxidation of cyanide in aqueous solution and industrial wastewater. *Chem. Eng. J.* **2018**, *350*, 673–680. [CrossRef]
11. Zhang, Y.C.; Zhang, Q.; Hong, J.M. Sulfate radical degradation of acetaminophen by novel iron–copper bimetallic oxidation catalyzed by persulfate: Mechanism and degradation pathways. *Appl. Surf. Sci.* **2017**, *422*, 443–451. [CrossRef]
12. Li, M.X.; Sun, J.F.; Han, D.D.; Wei, B.; Mei, Q.; An, Z.X.; Wang, X.Y.; Cao, H.J.; Xie, J.; He, M.X. Theoretical investigation on the contribution of HO•, $SO_4^{\bullet-}$ and $CO_3^{\bullet-}$ radicals to the degradation of phenacetin in water: Mechanisms, kinetics, and toxicity evaluation. *Ecotoxicol. Environ. Saf.* **2020**, *204*, 110977. [CrossRef]
13. Xiao, R.Y.; He, L.; Luo, Z.H.; Spinney, R.; Wei, Z.S.; Dionysiou, D.D.; Zhao, F.P. An experimental and theoretical study on the degradation of clonidine by hydroxyl and sulfate radicals. *Sci. Total Environ.* **2020**, *710*, 136333. [CrossRef]
14. Devi, P.; Das, U.; Dalai, A.K. In-situ chemical oxidation: Principle and applications of peroxide and persulfate treatments in wastewater systems. *Sci. Total Environ.* **2016**, *571*, 643–657. [CrossRef]
15. Ghanbari, F.; Moradi, M. Application of peroxymonosulfate and its activation methods for degradation of environmental organic pollutants: Review. *Chem. Eng. J.* **2017**, *310*, 41–62. [CrossRef]
16. Tong, X.; Wang, S.N.; Wang, L.M. Kinetics and mechanism of syringic acid degradation initiated by hydroxyl radical and sulphate radical in the aqueous phase. *Chemosphere* **2020**, *256*, 126997. [CrossRef]

17. Gao, L.W.; Mao, Q.M.; Luo, S.; Cao, L.Y.; Xie, X.D.; Yang, Y.; Deng, Y.F.; Wei, Z.S. Experimental and theoretical insights into kinetics and mechanisms of hydroxyl and sulfate radicals-mediated degradation of sulfamethoxazole: Similarities and differences. *Environ. Pollut.* **2020**, *259*, 113795. [CrossRef]
18. Wang, S.L.; Wu, J.F.; Lu, X.Q.; Xu, W.X.; Gong, Q.; Ding, J.Q.; Dan, B.S.; Xie, P.C. Removal of acetaminophen in the Fe^{2+}/persulfate system: Kinetic model and degradation pathways. *Chem. Eng. J.* **2019**, *358*, 1091–1100. [CrossRef]
19. Li, B.Q.; Ma, X.Y.; Deng, J.; Li, Q.S.; Chen, W.Z.; Li, G.X.; Chen, G.Y.; Wang, J.P. Comparison of acetaminophen degradation in UV-LED-based advance oxidation processes: Reaction kinetics, radicals contribution, degradation pathways and acute toxicity assessment. *Sci. Total Environ.* **2020**, *723*, 137993. [CrossRef] [PubMed]
20. Li, H.X.; Miao, X.R.; Zhang, J.; Du, J.; Xu, S.D.; Tang, J.H.; Zhang, Y.Y. DFT studies on the reaction mechanism and kinetics of dibutyl phthalate initiated by hydroxyl and sulfate radicals: Prediction of the most reactive sites. *Chem. Eng. J.* **2020**, *381*, 122680. [CrossRef]
21. Liu, W.; Lv, G.C.; Sun, X.M.; He, L.; Zhang, C.X.; Li, Z.Q. Theoretical study on the reaction of anthracene with sulfate radical and hydroxyl radical in aqueous solution. *Ecotoxicol. Environ. Saf.* **2019**, *183*, 109551. [CrossRef]
22. Mei, Q.; Sun, J.F.; Han, D.D.; Wei, B.; An, Z.X.; Wang, X.Y.; Xie, J.; Zhan, J.H.; He, M.X. Sulfate and hydroxyl radicals-initiated degradation reaction on phenolic contaminants in the aqueous phase: Mechanisms, kinetics and toxicity assessment. *Chem. Eng. J.* **2019**, *373*, 668–676. [CrossRef]
23. Yang, J.X.; Lv, G.C.; Wang, Z.H.; Sun, X.M.; Gao, J. Mechanisms, kinetics and eco-toxicity assessment of singlet oxygen, sulfate and hydroxyl radicals-initiated degradation of fenpiclonil in aquatic environments. *J. Hazard. Mater.* **2021**, *409*, 124505. [CrossRef] [PubMed]
24. Hohenstein, E.G.; Chill, S.T.; Sherrill, C.D. Assessment of the performance of the M05-2X and M06-2X exchange-correlation functionals for noncovalent interactions in biomolecules. *J. Chem. Theory Comput.* **2008**, *4*, 1996–2000. [CrossRef] [PubMed]
25. Mardirossian, N.; Head-Gordon, M. Thirty years of density functional theory in computational chemistry: An overview and extensive assessment of 200 density functionals. *Mol. Phys.* **2017**, *115*, 2315–2372. [CrossRef]
26. Zhao, Y.; Truhlar, D.G. The M06 suite of density functionals for main group thermochemistry, thermochemical kinetics, noncovalent interactions, excited states, and transition elements: Two new functionals and systematic testing of four M06-class functionals and 12 other functionals. *Theor. Chem. Acc.* **2008**, *120*, 215–241. [CrossRef]
27. Yang, Z.H.; Su, R.H.; Luo, S.; Spinney, R.; Cai, M.Q.; Xiao, R.Y.; Wei, Z.S. Comparison of the reactivity of ibuprofen with sulfate and hydroxyl radicals: An experimental and theoretical study. *Sci. Total. Environ.* **2017**, *590*, 751–760. [CrossRef]
28. He, L.; Sun, X.M.; Zhu, F.P.; Ren, S.J.; Wang, S.G. OH-initiated transformation and hydrolysis of aspirin in AOPs system: DFT and experimental studies. *Sci. Total Environ.* **2017**, *592*, 33–40. [CrossRef]
29. Yao, J.F.; Tang, Y.Z.; Zhang, Y.J.; Ruan, M.; Chen, F.; Wu, W.Z.; Sun, J.Y. Quantum chemical study of the mechanisms, kinetics, and ecotoxicity assessment of OH radical-initiated reactions of 2, 2′, 4, 4′, 5, 5′-hexabrominated diphenyl ether (BDE-153) in atmosphere and wastewater. *Chem. Eng. J.* **2021**, *422*, 129916. [CrossRef]
30. Zou, M.T.; Qi, Y.M.; Qu, R.J.; Al-Basher, G.; Pan, X.X.; Wang, Z.Y.; Huo, Z.L.; Zhu, F. Effective degradation of 2,4-dihydroxybenzophenone by zero-valent iron powder (Fe^0)-activated persulfate in aqueous solution: Kinetic study, product identification and theoretical calculations. *Sci. Total Environ.* **2021**, *771*, 144743. [CrossRef]
31. Frisch, M.J.; Trucks, G.W.; Schlegel, H.B.; Scuseria, G.E.; Robb, M.A.; Cheeseman, J.R.; Scalmani, V.; Barone, G.A.; Petersson, H.; Nakatsuji, X.; et al. *Gaussian 16 (Revision A.03)*; Gaussian, Inc.: Pittsburgh, PA, USA, 2016.
32. Maeda, S.; Harabuchi, Y.; Ono, Y.; Taketsugu, T.; Morokuma, K. Intrinsic reaction coordinate: Calculation, bifurcation, and automated search. *Int. J. Quant. Chem.* **2015**, *115*, 258–269. [CrossRef]
33. Marenich, A.V.; Cramer, C.J.; Truhlar, D.G. Universal solvation model based on solute electron density and on a continuum model of the solvent defined by the bulk dielectric constant and atomic surface tensions. *J. Phys. Chem. B* **2009**, *113*, 6378–6396. [CrossRef] [PubMed]
34. Canneaux, S.; Bohr, F.; Henon, E. KiSThelP: A program to predict thermodynamic properties and rate constants from quantum chemistry results. *J. Comput. Chem.* **2014**, *35*, 82–93. [CrossRef] [PubMed]
35. Altarawneh, M.; Dlugogorski, B.Z. Formation and chlorination of carbazole, phenoxazine, and phenazine. *Environ. Sci. Technol.* **2015**, *49*, 2215–2221. [CrossRef]
36. Wang, X.Y.; Sun, J.F.; Han, D.D.; Bao, L.; Mei, Q.; Wei, B.; An, Z.X.; He, M.X.; Yuan, S.L.; Xie, J.; et al. Gaseous and heterogeneous reactions of low-molecular-weight (LMW) unsaturated ketones with O_3: Mechanisms, kinetics, and effects of mineral dust in tropospheric chemical processes. *Chem. Eng. J.* **2020**, *395*, 125083. [CrossRef]
37. Yao, J.F.; Sun, Y.N.; Tang, Y.Z.; Zhang, Y.J.; Wu, W.Z.; Sun, J.Y. Atmospheric oxidation of 4-(2-methoxyethyl) phenol initiated by OH radical in the presence of O_2 and NO_x: A mechanistic and kinetic study. *Int. J. Quantum. Chem.* **2021**, *121*, e26650. [CrossRef]
38. An, Z.X.; Sun, J.F.; Han, D.D.; Mei, Q.; Wei, B.; Wang, X.Y.; He, M.X. Theoretical study on the mechanisms, kinetics and ecotoxicity assessment of OH-initiated reactions of guaiacol in atmosphere and wastewater. *Sci. Total Environ.* **2019**, *685*, 729–740. [CrossRef]
39. Ji, Y.M.; Zhao, J.; Terazono, H.; Misawa, K.; Levitt, N.P.; Li, Y.X.; Lin, Y.; Peng, J.F.; Wang, Y.; Duan, L.; et al. Reassessing the atmospheric oxidation mechanism of toluene. *Proc. Natl. Acad. Sci. USA* **2017**, *114*, 8169–8174. [CrossRef]
40. Collins, F.C.; Kimball, G.E. Diffusion-controlled reaction rates. *J. Colloid Sci.* **1949**, *4*, 425–437. [CrossRef]
41. Steubing, W. Ueber die von der molekularkinetischen Theorie der Wärme geforderte Bewegung von in Flüssigkeiten suspendierten Teilchen. *Z. Chem. Ind. Kolloide* **1908**, *3*, 230. [CrossRef]

42. ECOSAR v2.0. Available online: https://www.epa.gov/oppt/newchems/tools/21ecosar.htm (accessed on 1 January 2017).
43. Bai, F.Y.; Ni, S.; Tang, Y.Z.; Pan, X.M.; Zhao, Z. Ciprofloxacin transformation in aqueous environments: Mechanism, kinetics, and toxicity assessment during OH-mediated oxidation. *Sci. Total. Environ.* **2020**, *699*, 134190. [CrossRef]
44. Shada, A.; Chen, J.; Qu, R.J.; Dar, A.A.; Bin-Jumah, M.; Allam, A.A.; Wang, Z.Y. Degradation of sulfadimethoxine in phosphate buffer solution by UV alone, UV/PMS and UV/H_2O_2: Kinetics, degradation products, and reaction pathways. *Chem. Eng. J.* **2020**, *398*, 125357. [CrossRef]
45. Chen, J.; Xu, X.X.; Zeng, X.L.; Feng, M.B.; Qu, R.J.; Wang, Z.Y.; Nesnas, N.; Sharma, V.K. Ferrate(VI) oxidation of polychlorinated diphenyl sulfides: Kinetics, degradation, and oxidized products. *Water Res.* **2018**, *143*, 1–9. [CrossRef] [PubMed]
46. Shiroudi, A.; Deleuze, M.S.; Canneaux, S. Theoretical study of the oxidation mechanisms of naphthalene initiated by hydroxyl radicals: The O_2 addition reaction pathways. *Phys. Chem. Chem. Phys.* **2015**, *17*, 13719–13732. [CrossRef] [PubMed]
47. Li, M.X.; Sun, J.F.; Mei, Q.; Wei, B.; An, Z.X.; Cao, H.J.; Zhang, C.; Xie, J.; Zhan, J.H.; Wang, W.X.; et al. Acetaminophen degradation by hydroxyl and organic radicals in the peracetic acid-based advanced oxidation processes: Theoretical calculation and toxicity assessment. *J. Hazard. Mater.* **2021**, *416*, 126250. [CrossRef] [PubMed]